ACS Sustainable Chemistry & Engineering

pubs.acs.org/journal/ascecg

Research Article

Open Access

This article is licensed under CC-BY-NC-ND 4.0

Direct Conversion of CO_2 to Olefins over a Cr_2O_3/ZSM-5@CaO Cooperative and Bifunctional Material Under Isothermal Conditions

Khaled Baamran and Ali A. Rownaghi*

Cite This: *ACS Sustainable Chem. Eng.* 2024, 12, 17783−17792

Read Online

ACCESS | Metrics & More | Article Recommendations | Supporting Information

ABSTRACT: Direct conversion of point-source CO_2 into fine chemicals over cooperative and bifunctional materials (BFMs) − composed of adsorbents and catalysts − has emerged as a promising approach to improve the energy efficiency of the carbon capture and conversion processes. In this study, a bifunctional material consisting of Cr_2O_3/ZSM-5 catalyst and CaO adsorbent was developed and tested in the CO_2-oxidative dehydrogenation of propane (CO_2−ODHP) for reactive capture of CO_2 in a fixed bed reactor. First, CaO was prepared using two distinct methods: solid-state and citrate sol−gel. The citrate sol−gel method resulted in small and finely-distributed CaO particles, allowing more accessible sites for CO_2 adsorption. Consequently, a high CO_2 adsorption capacity of ∼14 mmol/g was achieved with fast adsorption kinetics compared to CaO prepared by the solid-state method. The CaO adsorbent was then combined with the Cr_2O_3/ZSM-5 catalyst for BFM synthesis and tested in the CO_2−ODHP process, targeting propylene production. The BFM was extensively characterized to provide insights into the BFM's surface chemistry, morphology, and reaction mechanism in the reactive capture process of CO_2−ODHP. The results revealed that under isothermal adsorption−reaction conditions at 600 °C, a propane conversion of 22.5%, a propylene selectivity of 55.3%, and an olefin selectivity of 67.3% were achieved. The excellent propylene selectivity was attributed to the catalyst acidity and redox property of the Cr_2O_3/ZSM-5 catalyst, which facilitated the reaction pathway of propane dehydrogenation in the process of CO_2−ODHP. Overall, this study renders Cr_2O_3/ZSM-5@CaO as promising BFMs with high CO_2 capture capacity and catalytic activity for integrated CO_2 capture and conversion in the ODHP reaction.

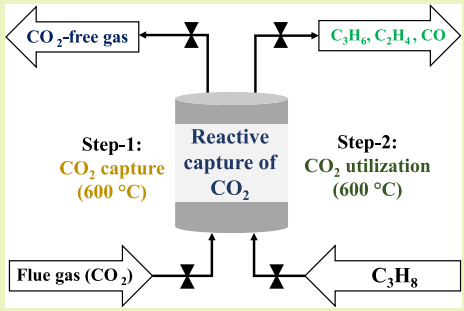

KEYWORDS: *point source carbon capture, cooperative and bifunctional materials, reactive capture, olefin formation*

1. INTRODUCTION

The urgent need to address climate change has driven innovations in CO_2 capture technologies and researchers around the world have been actively seeking innovative solutions to manage atmospheric CO_2 emissions. CO_2 capture by amine scrubbing is an industrial benchmark process currently implemented worldwide, but it has faced critical challenges due to its inherent energy-intensive and resource-consuming nature, without providing significant economic returns. As a result, alternative CO_2 management strategies are being actively explored to address these limitations. Among various capture approaches investigated to date, adsorption has emerged as a promising option due to its low energy requirements and minimal environmental footprint. However, the long-term viability of this approach hinges on effective CO_2 management.[1−7]

Leveraging CO_2 as a feedstock in beneficial chemical processes, such as employing CO_2 as a mild oxidant for the oxidative dehydrogenation of ethane and propane and transforming CO_2 into CO—a crucial intermediate for synthetic fuel production—offers significant potential.[8−10] Current carbon-capture-conversion processes are implemented sequentially, with adsorption and reaction occurring in separate columns, making the process energy-intensive due to significant thermal gradients.[11−18] The significant thermal gradients between the two processes lead to lengthy cycle times, low productivity, and substantial energy expenditures. To address these challenges, innovative process integrations or novel materials that can efficiently merge adsorption and catalysis are being explored.[15,19,20]

Recently, researchers have developed innovative bifunctional materials (BFMs) that combine two critical properties: high-temperature CO_2 adsorption and heterogeneous catalysis. These BFMs, such as CaO, K−Ca and metal-oxide composites, can efficiently capture and convert CO_2 at elevated temperatures. For example, K−Ca/Cr_2O_3-ZSM-5 and CaO/Cr_2O_3-ZSM-5 BFMs have been developed for single-bed CO_2 adsorption and utilization in the ethane oxidative dehydrogenation reaction.[15] Similarly, Farrauto[26−30] and colleagues have

Received: August 19, 2024
Revised: October 21, 2024
Accepted: October 22, 2024
Published: November 20, 2024

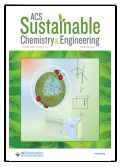

ACS Publications

© 2024 The Authors. Published by American Chemical Society

developed CaO/Al_2O_3 with various metal incorporations for methane reforming applications.[22−25]

These advancements in BFMs development pave the way for more efficient and integrated CO_2 capture-utilization processes, such as the CO_2-oxidative dehydrogenation of propane (CO_2−ODHP). We have previously demonstrated this concept in reactive capture of CO_2−ODHP process.[7,31] However, previous studies focused on screening ZSM-5 zeolite incorporating several metal oxides such as V, Cr, and Ce, but lacked insights into the reaction mechanism of the integrated CO_2−ODHP process.[21] Among these catalysts investigated, Cr-based catalysts displayed promising results due to redox properties of the chromium oxide, which enhance catalyst acidity. These capabilities, stemming from its high oxidation states such as Cr^{6+} and Cr^{3+}, facilitate the Mars-van Krevelen (MvK) mechanism.[9,32] To enable high stability of the Cr catalyst, Cr is supported by high surface area materials such as zeolites, which can provide a special environment (e.g., channel confinement effects, acidic sites, and electron transfer) for catalytic reactions. Among the investigated zeolites, ZSM-5 with Si/Al = 280 exhibited high catalytic performance in the dehydrogenation reactions. Based on the literature suggestions, high-silica ZSM-5 zeolite reduces Brønsted acidity, which is advantageous in this case for minimizing unwanted cracking and side reactions. This in turn, selectively promotes the dehydrogenation of propane to propylene while minimizing excessive byproduct formation.[33,34]

Motivated by this need, a BFM consisting of CaO—prepared by a citrate sol−gel method—and Cr_2O_3/ZSM-5 was developed and tested in the CO_2−ODHP process. The BFM was extensively characterized to provide insights into the BFM's surface chemistry, morphology, and reaction mechanism in the reactive capture process of CO_2−ODHP. The findings from the dynamic experiments indicated the possibility of *in situ* CO_2 conversion during the ODHP reaction under isothermal conditions of 600−600 °C for adsorption−reaction, providing high olefin selectivity. These findings, under the applied process conditions, also confirm the important role of CO_2 as a mild oxidant, which favors the reaction pathway of propane dehydrogenation into olefins.

2. EXPERIMENTAL SECTION

2.1. Materials. The following materials were used for the BFM synthesis without further purification: chromium(III) nitrate nonahydrate ($Cr(NO_3)_3{\cdot}9H_2O$) (99%, Sigma-Aldrich), calcium carbonate ($CaCO_3$) (99%, Sigma-Aldrich), calcium nitrate tetrahydrate ($Ca(NO_3)_2{\cdot}4H_2O$) (≥99%, Sigma-Aldrich), ZSM-5 (SiO_2:Al_2O_3 ratio = 280, Zeolyst International), and citric acid (≥99.5%, ACS reagent, Sigma-Aldrich). All ultrahigh purity (UHP) gases used in this study were purchased from Airgas.

2.2. Adsorbent Synthesis. The CaO adsorbent was synthesized using two different methods: the solid-state method and the citrate sol−gel method. For the solid-state method, CaO (CaO-ss) was prepared by calcining $CaCO_3$ at 700 °C for 5 h, using a heating ramp of 5 °C/min. In the citrate sol−gel method, and citric acid were used as the calcium precursor and gelling agent, respectively.[35] Initially, 2.36 g of $Ca(NO_3)_2{\cdot}4H_2O$ and 5.76 g of citric acid were dispersed in 50 mL of deionized water. The mixture was then stirred at 400 rpm and 150 °C until gelation formed. The resulting gel was transferred to an oven and dried at 120 °C for 24 h. Finally, the dried gel was ground into a homogeneous powder using a mortar and pestle and then calcined at 800 °C for 6 h under static air conditions using a heating rate of 5 °C/min. The CaO prepared by this method is referred to as CaO-sg.

2.3. Catalyst/BFM Synthesis. For the synthesis of the Cr_{10}/ZSM-5 catalyst (where 10 refers to the inclusion of 10 wt % chromium precursor in the catalyst sample), the wet impregnation method was used, which involved the incorporation of the chromium precursor into the ZSM-5 zeolite. Briefly, 10 wt % of $Cr(NO_3)_3{\cdot}9H_2O$ was dissolved in 50 mL of ZSM-5 solution and stirred at 400 rpm for 1 h. The resulting slurry was dried at 120 °C for 24 h, ground into a homogeneous powder using a mortar and pestle, and then calcined at 700 °C for 5 h with a heating rate of 5 °C/min before being used in experiments. For the synthesis of BFMs, the synthesized Cr_{10}/ZSM-5 catalyst and CaO adsorbent were physically mixed to form three different compositions: $(Cr_{10}/ZSM\text{-}5)_{80}/(CaO)_{20}$, $(Cr_{10}/ZSM\text{-}5)_{50}/(CaO)_{50}$, and $(Cr_{10}/ZSM\text{-}5)_{20}/(CaO)_{80}$ in the powder form. The 50:50 mass composition appeared to offer an optimal balance of adsorption capacity, making it a suitable choice for BFM synthesis. In contrast, the 20:80 composition, which demonstrated the highest adsorption capacity, may reduce the catalytic activity. Therefore, the 50:50 composition was selected for reactive capture experiments (Figure S1c). The materials were labeled as BFM-A and BFM-B, which refer to different adsorbents (CaO-ss and CaO-sg) combined with the catalyst. BFM-A stands for the $(Cr_{10}/ZSM\text{-}5)_{50}/(CaO\text{-}ss)_{50}$, while BFM-B stands for the $(Cr_{10}/ZSM\text{-}5)_{50}/(CaO\text{-}sg)_{50}$.

2.4. Materials Characterization. The textural properties of the samples were evaluated by using nitrogen physisorption tests on a Micromeritics 3Flex gas analyzer at 77 K. Prior to the analysis, the samples were degassed at 250 °C for 1 h on a Micromeritics Smart VacPrep instrument. The pore size distribution and surface area were estimated by the nonlocal density functional theory (NLDFT) and the Brunauer−Emmett−Teller (BET) methods, respectively. Elemental dispersions of metals and surface morphology of the materials were investigated using scanning electron microscopy (SEM) with an FEI Quanta 600F SEM, equipped with an Oxford Inca X-act detector for energy-dispersive X-ray spectroscopy (EDX). The oxidation states of the elements were examined via X-ray photoelectron spectroscopy (XPS) on a PHI 5000 VersaProbe III scanning XPS microprobe (Physical Electronics, ULVAC-PHI Inc.), utilizing an Al Kα (1486.6 eV) radiation source and a hemispherical analyzer. All binding energies were calibrated to the adventitious carbon feature (C 1s) at 284.6 eV. The crystallinity of the developed BFMs was assessed using powder X-ray diffraction (XRD) patterns recorded on a PANalytical X'Pert Pro X-ray diffractometer with CuKα radiation (λ = 1.5418 Å). To evaluate the reducibility of the materials, hydrogen temperature-programmed reduction (H_2-TPR) was conducted on a 3Flex gas analyzer. Additionally, the catalytic acidity was determined by the temperature-programmed desorption of NH_3 (NH_3-TPD) on the same 3Flex instrument. As a complementary method to NH_3-TPD, pyridine-fourier transform infrared spectroscopy (Py-FTIR) was performed on a Nicolet iS50 FTIR instrument equipped with an attenuated total reflectance (ATR) diamond. Before characterization, samples were degassed under vacuum at 200 °C for 12 h to remove any preadsorbed species. Subsequently, the samples were sealed in glass jars with 10 mL of liquid pyridine and heated to 50 °C for 12 h to saturate the acid sites with pyridine vapor. An Agilent Cary 670 FTIR spectrometer was utilized to characterize the functional groups present in the materials. A Q500 thermogravimetric analyzer (TGA) from TA Instruments was used to evaluate CO_2 adsorption and analyze coke formation on the materials. For spent samples, heating was carried out under a N_2 flow of 100 mL/min at 700 °C, with a ramp rate of 10 °C/min.

2.5. In Situ CO_2/C_3H_8-DRIFTS Experiments. The reactivity of each BFM was assessed over a temperature range of 100 to 500 °C, both with and without the presence of CO_2, using diffuse reflectance infrared Fourier transform spectroscopy (DRIFTS). It should be noted that DRIFTS measurements were limited to 500 °C due to light interference at higher temperatures, which could compromise the reliability of data. Even though this temperature was lower than that used in the adsorption−reaction experiments, differences in the behavior of various BFMs were still observed, providing valuable insights into their performance across the tested temperature range.

https://doi.org/10.1021/acssuschemeng.4c06841
ACS Sustainable Chem. Eng. 2024, 12, 17783−17792

The experimental setup included a Nicolet iS-10 FTIR spectrometer (Thermo Fisher Scientific, Waltham, MA, USA) coupled to a catalytic reaction cell (Harrick Scientific, Pleasantville, NY, USA). Prior to analysis, the samples were heated in a flow of 120 mL/min helium to 500 °C and maintained at that temperature for 15 min. Subsequently, the samples were treated in a 50 mL/min mixture of 21% O_2/79% N_2. Following this, helium was reintroduced, and scans were conducted in helium at 500, 300, and 100 °C to obtain a suitable background spectrum. Next, a mixture of either 5% C_3H_8/95% N_2 or 5% C_3H_8/5% CO_2/90% N_2 was flowed at 100 mL/min, with scans taken at 100, 300, and 500 °C.

2.6. Carbon Capture and Utilization Experiments. The CO_2 capture capacity (mmol/g) was determined using TGA. Initially, each sample was degassed at 780 °C to activate the materials for 2 h, using a 100 mL/min flow rate of 100% N_2 at a heating rate of 10 °C/min. After the activation of the samples, the temperature was lowered to 650 °C and maintained for 2 h to ensure temperature stabilization. Then, the adsorption step was initiated using a 60 mL/min flow rate of 100% CO_2 for 1 h. The combined CO_2 capture and ODHP experiments were conducted in a fixed bed reactor, and the effluent product concentrations were monitored using a mass spectrometer. In a typical experiment, 0.25 g of BFM was placed in the middle of a quartz U-tube reactor (1 cm inner diameter), which was attached to a temperature-programmed gas analysis system (Micromeritics AutoChem 2950 HP) equipped with an in-line mass spectrometer (Pfeiffer Vacuum). The BFM was packed between two layers of quartz wool. The sample was first pretreated by heating at a rate of 10 °C/min from 25 to 700 °C for 1 h under a 30 mL/min flow rate of 100% Ar. Afterward, the bed was cooled to the adsorption temperature (600 °C), where 100% CO_2 was introduced into the reactor for 30 min (pulse experiments). Then, the CO_2 flow was terminated, the system was purged with Ar for 5 min, and 100% C_3H_8 was introduced into the system at 600 and 700 °C with a heating rate of 10 °C/min. The reaction step was continued for 1 h, and by the end of this step, one cycle of CO_2−ODHP was completed, as shown in Figure 1. It is important to mention that changing the reaction temperature or repeating the adsorption−reaction cycle requires conducting a separate CO_2−ODHP experiment, as outlined in Figure 1. Additionally, all adsorption−reaction experiments were carried out as pulse experiments. To ensure the accuracy of results, we ran for 20 pulses, integrated all peaks for a specific gas, and used the peak area for parameter calculation (Figure S3b). The estimated parameters such as C_3H_8 conversion, product selectivity, and carbon balance were estimated at each pulse (20 times) using eqs S1−S3, and the average value was reported. To validate the product selectivity, CO_2−ODHP experiments at 600−600 °C were conducted and products were analyzed using gas chromatography (GC), and the results are shown in Figure S3a. Products were collected in a Tedlar gastight bag and manually injected into a PerkinElmer Clarus 600 GC using gastight syringes (Vici Valco). The GC was equipped with a ShinCarbon ST packed column (Restek), and thermal conductivity and flame ionization detectors (TCD and FID).

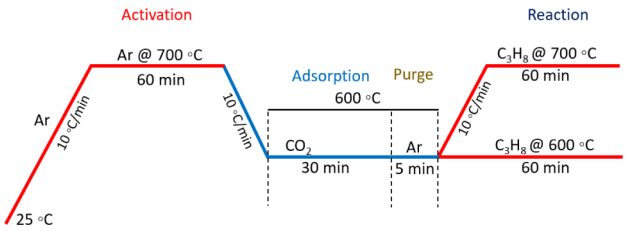

Figure 1. Schematic representation of the CO_2−ODHP adsorption−reaction process.

3. RESULTS AND DISCUSSION

Before initiating the reactive capture experiments, we focused on enhancing the CO_2 capture capacity by optimizing the synthesis conditions and employing two different synthesis methods—solid-state method and the citrate sol−gel—for CaO, as noted earlier. The CO_2 uptake over CaO-sg and CaO-ss adsorbents was evaluated by TGA, and as shown in Figure 2a, CaO-sg significantly outperformed CaO-ss, achieving ∼50% higher CO_2 uptake and faster adsorption kinetics.

To examine the enhanced CO_2 adsorption performance of CaO synthesized via the citrate sol−gel method, the SEM images of the samples' morphologies were obtained and are shown in Figure 3a−e. Although both synthesis methods

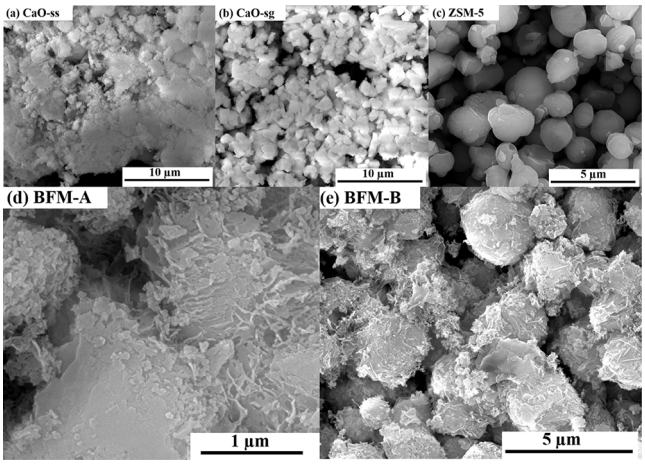

Figure 3. SEM images of (a) CaO-ss, (b) CaO-sg, (c) ZSM-5, (d) BFM-A, and (e) BFM-B.

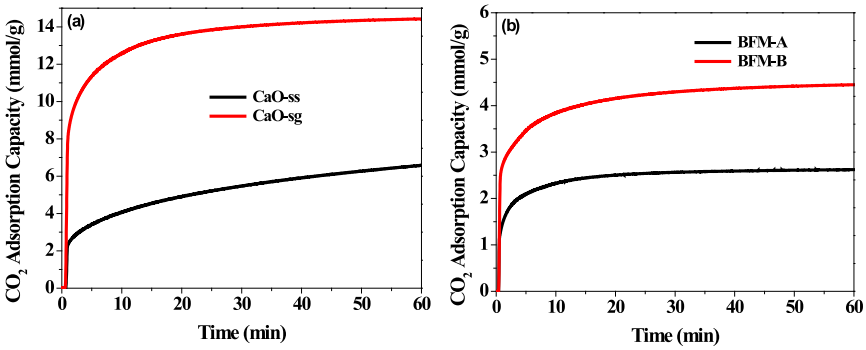

Figure 2. (a) CO_2 adsorption capacity (mmol/g) over CaO-ss and CaO-sg adsorbents; (b) CO_2 adsorption capacity (mmol/g) over BFM-A and BFM-B at 650 °C.

https://doi.org/10.1021/acssuschemeng.4c06841
ACS Sustainable Chem. Eng. 2024, 12, 17783−17792

produced CaO particles of similar size, there were notable differences in particle aggregation. The CaO prepared by the solid-state method (CaO-ss) showed significant agglomeration, forming large aggregates, while CaO from the citrate sol−gel method (CaO-sg) exhibited a well-dispersed particles distribution. These SEM images reveal that the severe aggregation in the CaO-ss sample resulted in larger particle clusters, whereas the sol−gel process minimized such aggregation. In the sol−gel method, citric acid complexes with calcium species to form a gel that uniformly confines the adsorbent precursor. Upon heating, the gel cracks and decomposes into smaller, more dispersed particles, resulting in finely distributed CaO particles with minimal aggregation, as observed in the CaO-sg sample.[35]

Both adsorbents, CaO-ss and CaO-sg, were blended with the Cr_2O_3/ZSM-5 catalyst to create a BFM for the reactive capture of CO_2 in the ODHP process. The SEM images of the as-prepared BFMs are shown in Figure 3, and the corresponding EDX spectra are shown in Figure S2. As anticipated, the CO_2 adsorption capacity was higher in Cr_2O_3/ZSM-5/CaO-sg (Figure 2b) due to the finely distributed small particles of CaO with minimal aggregation compared to Cr_2O_3/ZSM-5/CaO-ss, as evident from the SEM images (Figure 3d,e), discussed before. Consequently, the Cr_2O_3/ZSM-5/CaO-sg bifunctional material (BFM-B) was chosen for the reaction experiments due to its superior adsorption performance.

Figure 4 displays the FTIR spectra of the CaO adsorbents, Cr_2O_3/ZSM-5 catalyst, and the BFMs. Both CaO-ss and CaO-sg exhibited peaks at 700, 866, and 1400 cm^{-1}, corresponding to the stretching bands of $CaCO_3$. A small peak at 650 cm^{-1} indicated the CaO phase, and the appearance of a peak at 3637 cm^{-1} was due to the physisorption of water molecules.[36] The FTIR spectrum of Cr_2O_3/ZSM-5 showed strong peaks at 790 and 1068 cm^{-1}, which were characteristic of the ZSM-5 stretching bands.[37] Absorption bands at 547 cm^{-1} were linked to Cr−O bonds in the binding mode.[38] The FTIR spectra of the BFMs exhibited a combination of the stretching bands associated with both the CaO adsorbent and the Cr_2O_3/ZSM-5 catalyst, with a slight reduction in peak intensity observed due to the mixed phases.

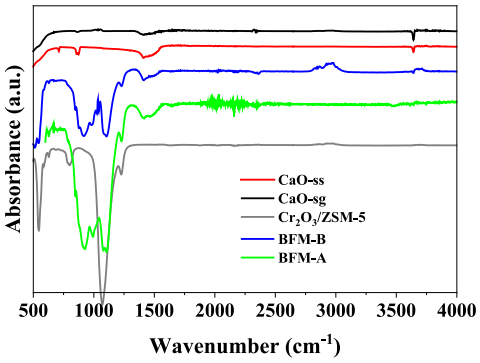

Figure 4. FTIR spectrum of adsorbents, catalyst, and BFMs.

The crystallinity of the CaO-sg adsorbent, Cr_2O_3/ZSM-5 catalyst, and BFM-B was evaluated using XRD, as shown in Figure S1a. The XRD pattern for CaO-sg displayed peaks at approximately 2θ = 33°, 38°, and 54°, corresponding to CaO. The XRD for Cr_2O_3/ZSM-5 revealed distinct peaks at 2θ = 7.8°, 8.9°, 23.1°, and 24.3°, which are characteristic of ZSM-5 and correspond to the (101), (020), (501), and (151) planes, respectively. The peaks for Cr_2O_3 were hard to observe, probably due to its amorphous structure. BFM-B exhibited a combination of CaO and the pristine catalyst with reduced peak intensity. Similar results were expected for BFM-A. Based on the data shown in Figure S1a, it was concluded that BFM-B is a composite material comprising Cr_2O_3/ZSM-5 and CaO, and that the crystallinity of the zeolite is preserved after incorporation of the CaO adsorbent.

The textural properties of the BFMs were evaluated by using N_2 physisorption, as shown in Figure S1b and Table S1. The physisorption profiles revealed that the BFMs exhibited Type II physisorption behavior with Type-H4 hysteresis, characteristic of microporous materials. This was anticipated, given ZSM-5's well-known microporous nature. The incorporation of Cr species and the addition of CaO did not significantly alter the primary microporous character of ZSM-5, but did reduce the surface area due to agglomeration resulting from the inclusion of adsorbents. However, the zeolite structure remained intact during the synthesis of the BFMs, as indicated by the shape of the hysteresis loop. This suggested that the BFMs preserved the zeolite's textural structure and likely their catalytic activity.

The XPS spectra of BFM-B are shown in Figure 5. The survey spectrum in Figure 5a displayed all of the orbital spins of the constituent elements, indicating that the incorporation of Cr_2O_3 and CaO species did not alter the interfacial structure of the zeolite. The main elements in ZSM-5, such as Si and Al, were still present, consistent with the XRD data. Since the Cr species are crucial for the reaction due to their high ion states, a high-resolution scan of Cr was performed, and the results are presented in Figure 5b. Peaks at approximately 588 and 578 eV correspond to the Cr $2p_{3/2}$ and Cr $2p_{1/2}$ orbitals, indicating the presence of Cr^{6+} and Cr^{3+} ion states.[37] The reduction of these ion states during the reaction is essential for lowering the energy barrier and tuning the reaction pathways in the CO_2−ODHP process.

To understand the changes in Cr species, the Cr $2p_{3/2}$ and Cr $2p_{1/2}$ peaks were analyzed, as depicted in Figure 5b. The intensities of these peaks and the Cr^{6+}/Cr^{3+} ratios are detailed in Table 1. It is known that Cr^{3+} species are crucial as they act as the active sites in Cr-based catalysts and contribute to the production of olefins through the alkane dehydrogenation reactions. In contrast Cr^{6+} species mainly serve as precursors to Cr^{3+}. Interestingly, the ratio of Cr^{6+}/Cr^{3+} was higher than 1 in the BFM-B, implying that the reduction property of the catalyst was not adversely affected by the inclusion of CaO. Furthermore, as summarized in Table 2, O_{ads} species were observed to be more abundant than O_{latt}, as indicated by the O_{ads}/O_{latt} ratio, which promotes high selectivity in dehydrogenation reactions leading to olefin formation.[39]

The redox properties of BFM-B were investigated using H_2-TPR, as shown in Figure 5d. Unlike ZSM-5/CaO-sg, which showed no reductive behavior, BFM-B exhibited significant reduction peaks at 341.5 and 599 °C, with a shoulder observed between 400 and 500 °C. These peaks corresponded to the reduction of chromium species, specifically, the conversion of Cr^{6+} to Cr^{3+} and Cr^{3+} to Cr^{2+}. This suggests that the propane conversion and olefin selectivity in the CO_2−ODHP process are driven by the Cr species, with the zeolite acting as a support to enhance the dispersion of the active species and facilitate the dehydrogenation of propane due to the acidic properties of ZSM-5.

https://doi.org/10.1021/acssuschemeng.4c06841
ACS Sustainable Chem. Eng. 2024, 12, 17783−17792

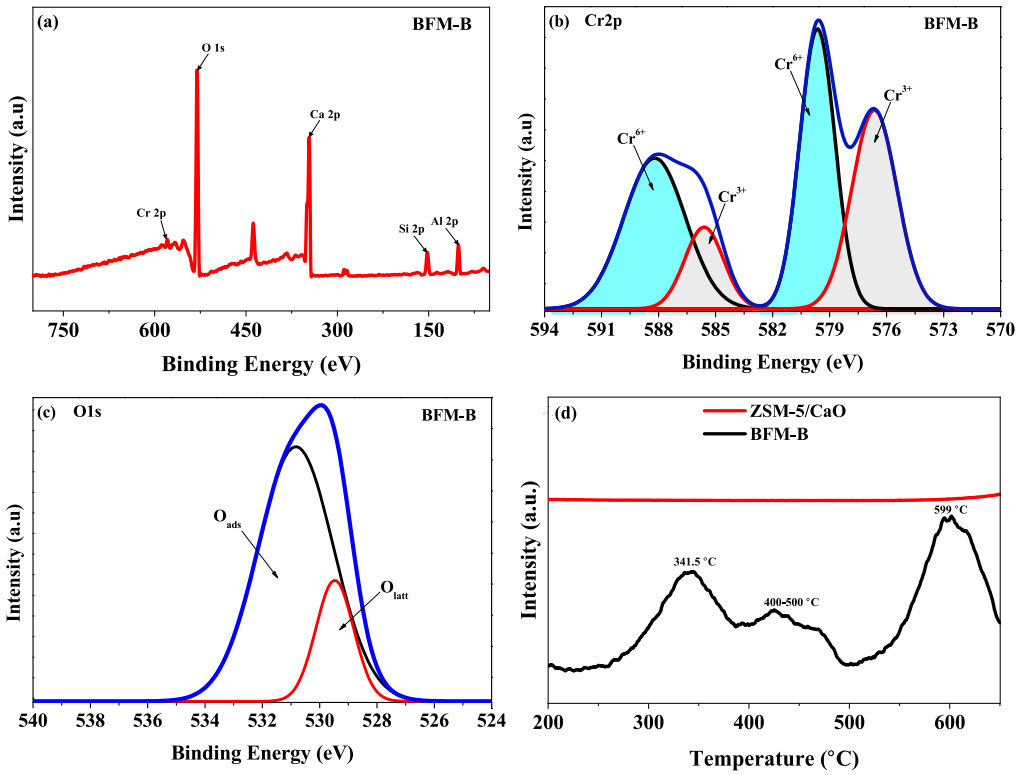

Figure 5. High-resolution XPS spectrum of the BFM-B (a) spectrum survey, (b) Cr 2p, (c) O 1s, and (d) H_2-TPR of the ZSM-5/CaO-sg and BFM-B.

Table 1. XPS Results of Curve Fitting on Cr 2p Binding Energies and Their Corresponding Species for BFM-B

	Cr $2p_{3/2}$				Cr $2p_{1/2}$			
sample	species	BE (eV)	peak intensity $\times 10^{-3}$	Cr^{6+}/ Cr^{3+} ratio	species	BE (eV)	peak intensity $\times 10^{-4}$	Cr^{6+}/ Cr^{3+} ratio
BFM-B	Cr^{6+}	588.2	2.17	2.78	Cr^{6+}	579.6	2.22	1.07
	Cr^{3+}	585.6	0.78		Cr^{3+}	576.6	2.07	

Table 2. XPS Results of Curve Fitting on O 1s Binding Energies and Their Corresponding Species for BFM-B

	O 1s			
sample	species	BE (eV)	peak intensity $\times 10^{-5}$	O_{ads}/O_{latt}
BFM-B	O_{latt}	529.5	1.4	2.07
	O_{ads}	530.8	2.9	

The acidity of the catalyst plays a crucial role in the CO_2−ODHP process, as it influences the adsorption and activation of propane. Figure 6a,b show the quantification of acid sites using NH_3-TPD and their characterization by type using Py-FTIR, respectively. Both samples exhibited a combination of weak and strong acid sites, corresponding to ammonia desorption at approximately 187 and 649 °C. Notably, BFM-B demonstrated greater acidity than ZSM-5/CaO with a more than 49% increase in total acidity, as evidenced by the higher amount of ammonia desorption. This result was expected, given that Cr_2O_3 is a strong acid.[31] The increased acidity is advantageous for ODHP performance, as it enhances the

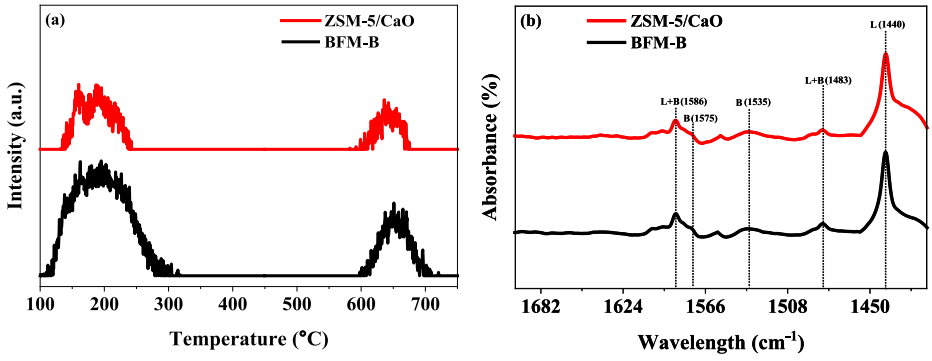

Figure 6. (a) NH_3-TPD profiles and (b) type of acid site characterized by Py-FTIR plots of ZSM-5/CaO-sg and the BFM-B.

https://doi.org/10.1021/acssuschemeng.4c06841
ACS Sustainable Chem. Eng. 2024, 12, 17783−17792

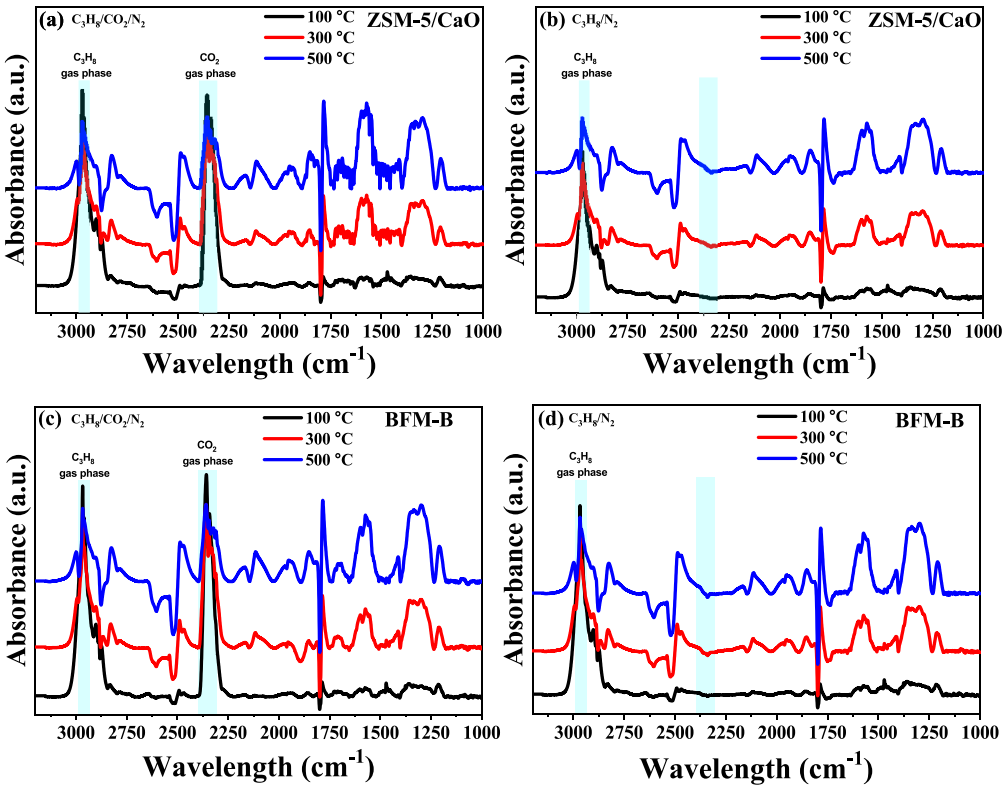

Figure 7. C_3H_8-DRIFTS profiles (a) ZSM-5/CaO-sg ($C_3H_8/CO_2/N_2$), (b) ZSM-5/CaO-sg (C_3H_8/N_2), (c) BFM-B ($C_3H_8/CO_2/N_2$), and (d) BFM-B (C_3H_8/N_2).

catalyst's ability to activate propane with a lower energy requirement.

The type of acid sites is as crucial as the acid density because it determines the overall dehydrogenation/cracking behavior, thereby affecting selectivity of products. The Py-FTIR spectra (Figure 6b) indicated that both samples contained a mixture of Lewis and Brønsted acid sites, with a predominance of Lewis sites, as evidenced by the strong peak at 1440 cm^{-1}. This dominant Lewis acidity was expected because ZSM-5, the catalyst support, is known for its Lewis acid sites. The Brønsted acid sites likely originate from isolated protons or hydroxyl groups in the zeolite framework. When Cr species were incorporated in BFM-B, there was no significant change in the acid type. This suggests that Cr species contributed to the overall quantity of acidity (Figure 6a), which is important for effectively activating and dehydrogenating propane.[31,40]

The reactive behavior of ZSM-5/CaO-sg and BFM-B samples was assessed by C_3H_8-DRIFTS with and without CO_2 from 100 to 500 °C to determine how temperature, CO_2, and Cr incorporation affected the ODHP reaction. The DRIFTS spectra of the ZSM-5/CaO-sg sample with $C_3H_8/CO_2/N_2$ (Figure 7a) and C_3H_8/N_2 (Figure 7b) showed notable differences due to the presence or absence of CO_2. At 100 °C, both sets of conditions exhibited minimal activity with weak peaks, indicating limited activation of propane. As the temperature increased to 300 and 500 °C, significant changes were observed. In both conditions, the peaks in the 3080−3000 cm^{-1} region, corresponding to the C═H stretching vibrations of alkenes, suggested the dehydrogenation of propane. The 2900−2800 cm^{-1} region showed strong peaks related to the gas-phase C−H stretching of propane. A notable peak at 2300 cm^{-1} under the $C_3H_8/CO_2/N_2$ conditions was attributed to gas-phase CO_2, which was absent under the C_3H_8/N_2 conditions. In the 2200−1650 cm^{-1} region, increasing intensity indicated the formation of oxygenated intermediates (C−O). The peaks at 1680−1600 cm^{-1} can be assigned to additional alkene species (C═C). The peaks at 1590 and 1456 cm^{-1} under the $C_3H_8/CO_2/N_2$ conditions suggested the presence of formate and carbonate species, whereas the 1400−1100 cm^{-1} peaks was attributed to carbonate species and C−O stretching in oxygenated intermediates.[41,42] It is also worth noting that the peak intensities at 2900−2800 and 2300 cm^{-1} for the reactant gas phase were reduced with increasing temperature, while the other peaks associated with formate, carbonyl, alkene, and carbonate species increased in intensity. This implied the conversion of reactants (propane and CO_2, or propane) due to the acidic sites of ZSM-5 and thermal activation of reactants at 100−500 °C.

Although the temperature range used in the DRIFTS analysis was relatively low for thermal catalysis of CO_2−ODHP, the peaks attributed to CO (2113 cm^{-1}) and carbonate species formation became slightly more intense in the presence of CO_2. The increased peak intensity of CO suggests the conversion of CO_2 into CO in the ODHP and RWGS reactions, while the peaks attributed to the carbonates could indicate residuals of CO_2 on CaO during adsorption. In the absence of CO_2, the acidic sites of ZSM-5 and the thermal activation of propane lead to the formation of CO and other intermediates/products.

The DRIFTS spectra of BFM-B with $C_3H_8/CO_2/N_2$ (Figure 7c) and C_3H_8/N_2 (Figure 7d) exhibited trends similar to those of the ZSM-5/CaO sample, indicating that Cr did not significantly impact catalytic activity within the temperature range of 100−500 °C. This temperature range is relatively low for the complete conversion of propane and CO_2, resulting in

https://doi.org/10.1021/acssuschemeng.4c06841
ACS Sustainable Chem. Eng. 2024, 12, 17783−17792

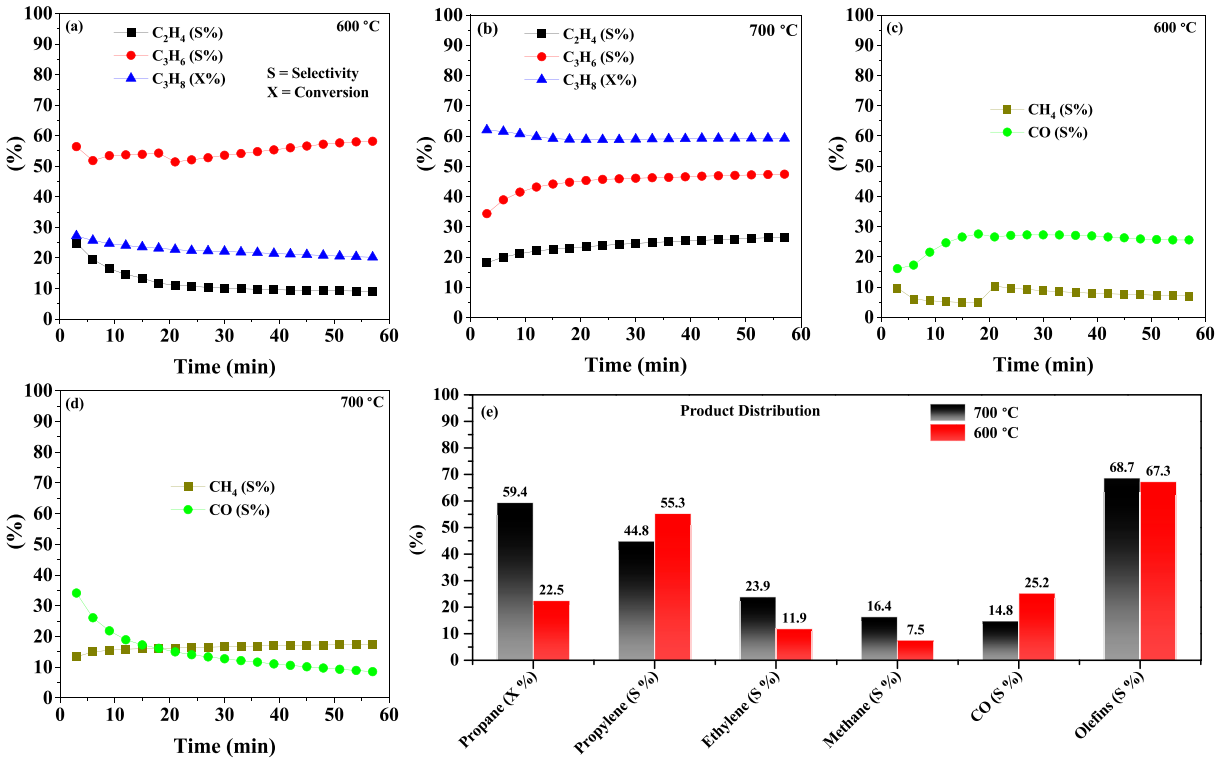

Figure 8. Catalytic performance of BFM-B showing (a) olefin selectivity and C_3H_8 conversion at 600 °C, (b) olefin selectivity and C_3H_8 conversion at 700 °C, (c) CH_4 and CO selectivity at 600 °C, (d) CH_4 and CO selectivity at 700 °C, and (e) product distribution at 600 and 700 °C.

only minor differences in catalytic activity after Cr incorporation. Cr species are more active at higher temperatures, which can significantly affect propane conversion and alkene selectivity due to their redox properties, as indicated by TPR analysis and mass spectrometry data during the actual adsorption−reaction experiments.

3.1. Direct Synthesis of Propylene from Propane over BFM. The synthesized BFM-B was evaluated for CO_2 capture-conversion through CO_2−ODHP under isothermal/semi-isothermal adsorption−reaction conditions. The adsorption−reaction results at 600−700 °C are shown in Figure 8a−e. Upon examining the catalytic results, the CO_2−ODHP experiments demonstrated excellent selectivity toward olefins with no noticeable catalyst deactivation during the 60 min reaction, as depicted in Figure 8a−e. At 600 °C, an increased selectivity for C_3H_6 and CO was observed, indicating two key reaction pathways. The higher propylene selectivity suggests that the oxidative dehydrogenation of propane is more efficient at this temperature. This is likely due to the enhanced catalytic activity at elevated temperatures, where the acidity of the catalyst promotes a more effective conversion of C_3H_8 to C_3H_6 through the dehydrogenation pathway. However, the CO_2−ODHP reaction at 600 °C can partially contribute to the production of CO.[43−45] Other reaction routes, such as reverse water gas shift (RWGS) and propane dry reforming (PDR) could produce CO at 600 °C, suggesting that the adsorbed CO_2 was likely converted in situ into CO due to the reaction with the released hydrogen during propane dehydrogenation in the RWGS or directly reacted with propane to form CO in the PDR.[32,46,47]

At 700 °C, there was a noticeable increase in the formation of ethylene and methane, indicating a tendency toward propane cracking. CO production was high in the early stages of the reaction but decreased gradually over time. This initial increase was likely due to the desorption of CO_2 when the reaction step was shifted to 700 °C, leading to a greater conversion of CO_2 to CO. Once CO_2 was consumed during the desorption/reaction step, CO level decreased due to the diminished presence of CO_2. As CO_2 was diminished, the propane cracking reaction became the favorable reaction due to the thermal activation of propane at 700 °C and catalyst activity.[7] Despite the tendency for propane cracking at 700 °C, total olefin selectivity was relatively reduced, as shown in Figure 8e. These findings underscore the important role of CO_2 as a mild oxidant in this chemical process, especially in facilitating pathways toward olefins.

To assess the stability of the developed BFM-B, four adsorption−reaction cycles were performed under isothermal conditions (600 °C for both adsorption and reaction), as shown in Figure S4a. The BFM-B exhibited good stability across the four cycles, with only a slight decrease in catalytic activity. For example, the C_3H_8 conversion and C_3H_6 selectivity decreased by approximately 9.2% and 16%, respectively. This suggested that operating at 600 °C resulted in minimal coke formation, which helped preserve the active sites. A cyclic CO_2 adsorption−desorption test was also conducted using 100% CO_2 (60 mL/min) for adsorption and 100% N_2 (100 mL/min) for desorption (regeneration) (Figure S4b). The results demonstrated that CaO-sg remained stable over seven cycles, with a slight reduction in CO_2 capacity of about 9.1%, indicating its suitability for use in developing reactive CO_2 capture materials for integrated capture and conversion processes.

In addition, our BFM-B showed performance comparable to that of materials reported in the literature for the CO_2-ODHP process. In particular, BFM-B exhibited good catalytic

https://doi.org/10.1021/acssuschemeng.4c06841
ACS Sustainable Chem. Eng. 2024, 12, 17783−17792

performance, achieving a C_3H_8 conversion of 22.5%, a C_3H_6 yield of 12.4%, and a C_3H_6 selectivity of 55.3% at 600 °C. This performance surpasses several reported CO_2−ODHP catalysts, including Fe_3Ni,[43] 4In/ZSM-5,[48] 7Ga/SiO_2−C,[49] 5Ga/ZrO_2,[50] and 12VO_x/AC.[51] However, BFM-B still falls short compared to other high-performing catalysts such as Cr-MSU-x28,[52] Cr_2O_3/ZrO_2,[53] and CrO/SiO_2.[54] Overall, the comparison of BFM-B with the catalysts listed in Table S2 emphasizes the potential of combining CO_2 capture and conversion over DFMs within a single reactor, while achieving competitive catalytic performance relative to that of conventional dehydrogenation catalysts.

The reaction mechanism for BFM-B in the CO_2−ODHP process involves the initial CO_2 capture by CaO to form $CaCO_3$. When propane is introduced to the catalyst surface at 600 °C, chromium species activate the C−H bonds in propane, and the catalyst's acidity facilitates the removal of hydrogen atoms, promoting the dehydrogenation pathway over cracking or other side reactions. Cr_2O_3 is known for its redox properties following the Mars-van Krevelen (MvK) mechanism, particularly cycling between Cr^{3+} and Cr^{6+} states due to the presence of the oxidant, adsorbed CO_2 in CaO in this case.[9,32] These redox cycles assist in the reoxidation of the catalyst and contribute to the production of propylene and CO. This mechanism facilitates the selective dehydrogenation of propane, as the reoxidation step helps regenerate active sites without excessive oxidation of propane. However, the RWGS, PDR, and the reverse Boudouard reactions can partially contribute to the production of CO.[9,32,55,56] At 700 °C, the same reaction mechanism is expected to occur, along with other side reactions, as indicated by the product distribution in Figure 8e. A higher dehydrogenation rate and propane cracking are observed, which can lead to the production of methane and ethylene. A summary of the possible reaction pathways is illustrated in Figure 9.

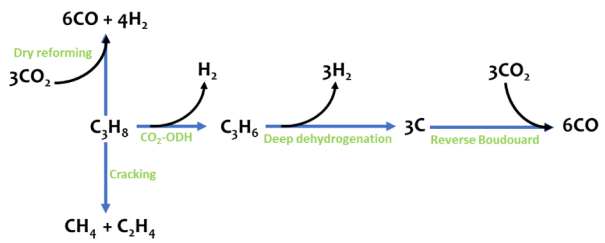

Figure 9. Possible reaction pathways involved in the CO_2−ODHP process.

Thermal decomposition analysis was conducted on the spent BFM-B samples at reaction temperatures of 600 and 700 °C, with the results shown in Figure 10. The TGA profiles revealed two main weight loss peaks: one around 430 °C, associated with the removal of water molecules, and another between 500 and 700 °C, linked to coke formation as indicative of a higher propensity for cracking reactions at this temperature.[37] The weight reduction for the spent sample at 700 °C was 13% greater compared to 600 °C. These findings suggested that for the BFM used in this study, a reaction temperature below 700 °C effectively reduces coke formation while maintaining propylene selectivity, as previously discussed.

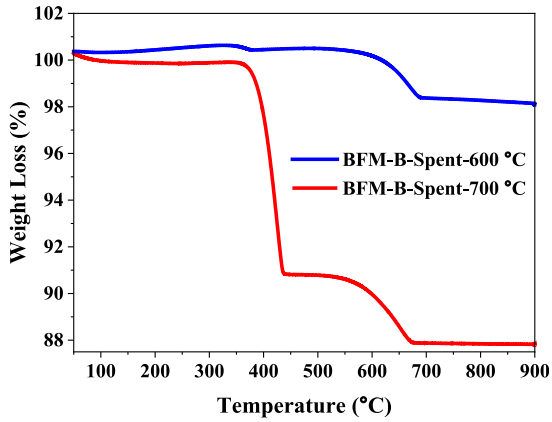

Figure 10. Thermal decomposition analysis of the spent BFM-B samples using TGA.

4. CONCLUSIONS

In this study, a bifunctional material comprising a Cr_2O_3/ZSM-5 catalyst and a CaO adsorbent was developed and evaluated for the CO_2−ODHP process in a fixed bed reactor, aiming at the reactive capture of CO_2 under isothermal conditions. Two methods were used to prepare CaO: solid-state and citrate sol−gel. The citrate sol−gel method produced small, well-distributed CaO particles, resulting in more accessible sites for CO_2 adsorption. This led to a high CO_2 adsorption capacity of approximately 14 mmol/g, with faster adsorption kinetics compared with CaO prepared by the solid-state method. Under isothermal adsorption−reaction conditions at 600 °C, the BFM achieved a propane conversion rate of 22.5% and a propylene selectivity of 55.3%. However, at 700 °C, cracking reactions became more favorable, reducing the overall olefin selectivity. The excellent olefin selectivity at lower temperatures was attributed to the catalyst's acidity and redox properties, which facilitated the propane dehydrogenation pathway in the CO_2−ODHP process. This study provides valuable insights into enhancing CO_2 adsorption capacity at high temperatures and developing efficient DFMs for integrated CO_2 capture-conversion processes.

■ ASSOCIATED CONTENT

Supporting Information

The Supporting Information is available free of charge at https://pubs.acs.org/doi/10.1021/acssuschemeng.4c06841.

Estimation of product distribution in CO_2-ODHP; XRD and BET data of adsorbents, catalyst, and BFMs; EDX analysis (mapping images and spectra); catalytic performance of BFM-B at 600 °C and stability performance of BFM-B and CaO adsorbent; comparison of BFM performance in CO_2-ODHP with the open literature; references (PDF)

■ AUTHOR INFORMATION

Corresponding Author

Ali A. Rownaghi − *United States Department of Energy, National Energy Technology Laboratory, Pittsburgh, Pennsylvania 15236, United States;* orcid.org/0000-0001-5228-5624; Email: ali.rownaghi@netl.doe.gov

https://doi.org/10.1021/acssuschemeng.4c06841
ACS Sustainable Chem. Eng. 2024, 12, 17783−17792

Author

Khaled Baamran − *United States Department of Energy, National Energy Technology Laboratory, Pittsburgh, Pennsylvania 15236, United States; NETL Support Contractor, Pittsburgh, Pennsylvania 15236, United States*

Complete contact information is available at: https://pubs.acs.org/10.1021/acssuschemeng.4c06841

Notes

This project was funded by the United States Department of Energy, National Energy Technology Laboratory, in part, through a site support contract. Neither the United States Government nor any agency thereof, nor any of their employees, nor the support contractor, nor any of their employees, makes any warranty, expressed or implied, or assumes any legal liability or responsibility for the accuracy, completeness, or usefulness of any information, apparatus, product, or process disclosed, or represents that its use would not infringe privately owned rights. Reference herein to any specific commercial product, process, or service by trade name, trademark, manufacturer, or otherwise does not necessarily constitute or imply its endorsement, recommendation, or favoring by the United States Government or any agency thereof. The views and opinions of authors expressed herein do not necessarily state or reflect those of the United States Government or any agency thereof.

The authors declare no competing financial interest.

■ ACKNOWLEDGMENTS

This work was performed in support of the U.S. Department of Energy's (DOE) Office of Fossil Energy and Carbon Management's Carbon Conversion Program and executed through the National Energy Technology Laboratory (NETL) Research & Innovation Center's Carbon Conversion Field Work Proposal. The authors want to thank Dr Sittichai Natesakhawat for his assistance with conducting reactive capture experiments (CO_2-C_3H_8), Dr Thuy Duong Nguyen Phan for her assistance with XPS/SEM analysis, Dr Ali K. Sekizkardes for his assistance with FTIR/BET analysis, Dr Bret Howard for his assistance with XRD analysis, Dr Eric Popczun for his assistance with TGA analysis, and Dr Christopher Marin for his assistance with GC analysis.

■ REFERENCES

(1) Baamran, K.; Lawson, S.; Rezaei, F.; Rownaghi, A. A. Reactive Carbon Capture: Cooperative and Bifunctional Adsorbent-Catalyst Materials and Process Integration for a New Carbon Economy. *Acc. Chem. Res.* **2024**, *57*, 2383.

(2) Al-Mamoori, A.; Krishnamurthy, A.; Rownaghi, A. A.; Rezaei, F. Carbon Capture and Utilization Update. *Energy Technol.* **2017**, *5* (6), 834−849.

(3) Gelles, T.; Krishnamurthy, A.; Adebayo, B.; Rownaghi, A. A.; Rezaei, F. Abatement of gaseous volatile organic compounds: A material perspective. *Catal. Today* **2020**, *350*, 3−18.

(4) Gelles, T.; Lawson, S.; Rownaghi, A. A.; Rezaei, F. Recent Advances in Development of Amine Functionalized Adsorbents for CO_2 Capture. *Adsorption* **2020**, *26*, 5−50.

(5) Riboldi, L.; Bolland, O. Overview on Pressure Swing Adsorption (PSA) as CO_2 Capture Technology: State-of-the-Art, Limits and Potentials. *Energy Proc.* **2017**, *114* (1876), 2390−2400.

(6) Aaron, D.; Tsouris, C. Separation of CO_2 from Flue Gas: A Review. *Sep. Sci. Technol.* **2005**, *40* (1−3), 321−348.

(7) Lawson, S.; Baamran, K.; Newport, K.; Garcia, E.; Jacobs, G.; Rezaei, F.; Rownaghi, A. A. Adsorption-Enhanced Bifunctional Catalysts for In Situ CO_2 Capture and Utilization in Propylene Production: A Proof-Of-Concept Study. *ACS Catal.* **2022**, *12* (22), 14264−14279.

(8) Rigamonti, M. G.; Shah, M.; Gambu, T. G.; Saeys, M.; Dusselier, M. Reshaping the Role of CO_2 in Propane Dehydrogenation: From Waste Gas to Platform Chemical. *ACS Catal.* **2022**, *12* (15), 9339−9358.

(9) Carter, J. H.; Bere, T.; Pitchers, J. R.; Hewes, D. G.; Vandegehuchte, B. D.; Kiely, C. J.; Taylor, S. H.; Hutchings, G. J. Direct and Oxidative Dehydrogenation of Propane: From Catalyst Design to Industrial Application. *Green Chem.* **2021**, *23* (24), 9747−9799.

(10) Xing, F.; Furukawa, S. Metallic Catalysts for Oxidative Dehydrogenation of Propane Using CO_2. *Chem. - Eur. J.* **2023**, *29* (3), No. e202202173.

(11) Atanga, M. A.; Rezaei, F.; Jawad, A.; Fitch, M.; Rownaghi, A. A. Oxidative Dehydrogenation of Propane to Propylene with Carbon Dioxide. *Appl. Catal., B* **2018**, *220*, 429−445.

(12) Lawson, S.; Li, X.; Thakkar, H.; Rownaghi, A. A.; Rezaei, F. Recent Advances in 3D Printing of Structured Materials for Adsorption and Catalysis Applications. *Chem. Rev.* **2021**, *121*, 6246.

(13) Lawson, S.; Farsad, A.; Adebayo, B.; Newport, K.; Schueddig, K.; Lowrey, E.; Polo-Garzon, F.; Rezaei, F.; Rownaghi, A. A. A Novel Method of 3D Printing High-Loaded Oxide/H-ZSM-5 Catalyst Monoliths for Carbon Dioxide Reduction in Tandem with Propane Dehydrogenation. *Adv. Sustain. Syst.* **2021**, *5*, 1−15.

(14) Lawson, S.; Newport, K. A.; Axtell, A.; Boucher, C.; Grant, B.; Haas, M.; Lee, M.; Rezaei, F.; Rownaghi, A. A. Structured Bifunctional Catalysts for CO_2 Activation and Oxidative Dehydrogenation of Propane. *ACS Sustainable Chem. Eng.* **2021**, *9*, 5716−5727.

(15) Al-Mamoori, A.; Lawson, S.; Rownaghi, A. A.; Rezaei, F. Oxidative Dehydrogenation of Ethane to Ethylene in an Integrated CO_2 Capture-Utilization Process. *Appl. Catal., B* **2020**, *278*, 119329.

(16) Sanz-Pérez, E. S.; Murdock, C. R.; Didas, S. A.; Jones, C. W. Direct Capture of CO_2 from Ambient Air. *Chem. Rev.* **2016**, *116* (19), 11840−11876.

(17) Koch, C.; Suhail, Z.; Goeppert, A.; Prakash, G. CO_2 Capture and Direct Air CO_2 Capture Followed by Integrated Conversion to Methane Assisted by Metal Hydroxides and a Ru/Al_2O_3 Catalyst. *ChemCatchem* **2023**, *15* (23), No. e202300877.

(18) Jeong-Potter, C.; Farrauto, R. Feasibility Study of Combining Direct Air Capture of CO_2 and Methanation at Isothermal Conditions with Dual Function Materials. *Appl. Catal., B* **2021**, *282*, 119416.

(19) Arellano-Treviño, M. A.; He, Z.; Libby, M. C.; Farrauto, R. J. Catalysts and Adsorbents for CO_2 Capture and Conversion with Dual Function Materials: Limitations of Ni-Containing DFMs for Flue Gas Applications. *J. CO_2 Util.* **2019**, *31* (March), 143−151.

(20) Omodolor, I. S.; Otor, H. O.; Andonegui, J. A.; Allen, B. J.; Alba-Rubio, A. C. Dual-Function Materials for CO_2 Capture and Conversion: A Review. *Ind. Eng. Chem. Res.* **2020**, *59* (40), 17612−17631.

(21) Lawson, S.; Baamran, K.; Newport, K.; Rezaei, F.; Rownaghi, A. A. Formulation and Processing of Dual Functional Adsorbent/Catalyst Structured Monoliths Using an Additively Manufactured Contactor for Direct Capture/Conversion of CO_2 with Cogeneration of Ethylene. *Chem. Eng. J.* **2022**, *431*, 133224.

(22) Baamran, K.; Lawson, S.; Rownaghi, A. A.; Rezaei, F. Process Evaluation and Kinetic Analysis of 3D-Printed Monoliths Comprised of CaO and Cr/H-ZSM-5 in Combined CO_2 Capture-C_2H_6 Oxidative Dehydrogenation to C_2H_4. *Chem. Eng. J.* **2022**, *435*, 134706.

(23) Baamran, K.; Lawson, S.; Rezaei, F.; Rownaghi, A. A. Reactive Capture and Conversion of CO_2 into Hydrogen over Bifunctional Structured $Ce_{1-x}Co_xNiO_3$/Ca Perovskite-Type Oxide Monoliths. *JACS Au* **2024**, *4*, 101−115.

(24) Lawson, S.; Baamran, K.; et al. Screening of Adsorbent/Catalyst Composite Monoliths for Carbon Capture-Utilization and Ethylene Production. *ACS Appl. Mater. Interfaces* **2021**, *13* (46), 55198−55207.

(25) Alghamdi, T.; Baamran, K. S.; Okoronkwo, M. U.; Rownaghi, A. A.; Rezaei, F. Metal-Doped K−Ca Double Salts with Improved

Capture Performance and Stability for High-Temperature CO_2 Adsorption. *Energy Fuels* **2021**, *35* (5), 4258−4266.
(26) Porta, A.; Visconti, C. G.; Castoldi, L.; Matarrese, R.; Jeong-Potter, C.; Farrauto, R.; Lietti, L. Ru-Ba Synergistic Effect in Dual Functioning Materials for Cyclic CO_2 Capture and Methanation. *Appl. Catal., B* **2021**, *283*, 119654.
(27) Duyar, M. S.; Trevino, M. A. A.; Farrauto, R. J. Dual Function Materials for CO_2 Capture and Conversion Using Renewable H_2. *Appl. Catal., B* **2015**, *168*, 370−376.
(28) Duyar, M. S.; Farrauto, R. J.; Castaldi, M. J.; Yegulalp, T. M. In Situ CO_2 Capture Using CaO/γ-Al_2O_3 Washcoated Monoliths for Sorption Enhanced Water Gas Shift Reaction. *Ind. Eng. Chem. Res.* **2014**, *53* (3), 1064−1072.
(29) Arellano-Treviño, M. A.; He, Z.; Libby, M. C.; Farrauto, R. J. Catalysts and Adsorbents for CO_2 Capture and Conversion with Dual Function Materials: Limitations of Ni-Containing DFMs for Flue Gas Applications. *J. CO_2 Util.* **2019**, *31*, 143−151.
(30) Arellano-Trevino, M. A.; Kanani, N.; Jeong-Potter, C. W.; Farrauto, R. J. Bimetallic Catalysts for CO_2 Capture and Hydrogenation at Simulated Flue Gas Conditions. *Chem. Eng. J.* **2019**, *375*, 121953.
(31) Lawson, S.; Baamran, K.; Newport, K.; Alghamadi, T.; Jacobs, G.; Rezaei, F.; Rownaghi, A. A. Integrated Direct Air Capture and Oxidative Dehydrogenation of Propane with CO_2 at Isothermal Conditions. *Appl. Catal., B* **2022**, *303*, 120907.
(32) Karakaya, C.; Kidder, M.; Wolden, C.; Kee, R. J.; Deutschmann, O. Mechanistic Interpretations and Insights for the Oxidative Dehydrogenation of Propane via CO_2 over Cr_2O_3/Al_2O_3 Catalysts. *Ind. Eng. Chem. Res.* **2022**, *61* (39), 14482−14493.
(33) Hu, Z. P.; Wang, Y.; Yang, D.; Yuan, Z. Y. CrO_x Supported on High-Silica HZSM-5 for Propane Dehydrogenation. *J. Energy Chem.* **2020**, *47*, 225−233.
(34) Zhai, S.; Xing, S.; Suo, Y.; Sun, M.; Chen, L.; Ren, J.; Liang, S.; Yuan, Z. Y. Boosting Propane Dehydrogenation Performance over the Highly Dispersed Co(II) Sites on Ultra-High Silica ZSM-5 Zeolite. *Fuel* **2024**, *366*, 131429.
(35) Yoon, H. J.; Lee, K. B. Introduction of Chemically Bonded Zirconium Oxide in CaO-Based High-Temperature CO_2 Sorbents for Enhanced Cyclic Sorption. *Chem. Eng. J.* **2019**, *355*, 850−857.
(36) Baamran, K.; Shareef, U.; Rezaei, F. Induction vacuum swing adsorption over magnetic sorbent monoliths and extrudates for ethylene/ethane separation. *AIchE J.* **2024**, *70*, No. e18401.
(37) Baamran, K.; Rownaghi, A. A.; Rezaei, F. Direct Synthesis of Ethylene and Hydrogen from CO_2 and Ethane over a Bifunctional Structured CaO/Cr_2O_3-V_2O_5/ZSM-5 Adsorbent/Catalyst Monolith. *ACS Sustainable Chem. Eng.* **2023**, *11* (3), 1006−1018.
(38) Tsegay, M. G.; Gebretinsae, H. G.; Nuru, Z. Y. Structural and Optical Properties of Green Synthesized Cr_2O_3 Nanoparticles. *Mater. Today Proc.* **2021**, *36*, 587−590.
(39) Li, Y.; Li, L.; Luo, S.; Huang, X.; Shen, J.; Jiang, C.; Jing, F. The Role of K in Tuning Oxidative Dehydrogenation of Ethane with CO_2 to Be Selective toward Ethylene. *Adv. Compos. Hybrid Mater.* **2021**, *4* (3), 793−805.
(40) Zhu, X.; Wang, H.; Wang, G.; Hou, Y.; Zhang, J.; Li, C.; Yang, C. Aromatization of N-Pentane over Zn/ZSM-5 Catalysts: Effect of Si/Al Ratio and Reaction Pathway. *J. Porous Mater.* **2021**, *28* (4), 1059−1067.
(41) Wu, R.; Liu, N.; Dai, C.; Yu, G.; Xu, R.; Chen, B. CO in Situ Directed Highly Efficient CrO_x@silicalite-1 for Propane Oxidation Dehydrogenation by CO_2. *Catal. Today* **2024**, *436*, 114746.
(42) Liu, J.; Wang, J.; Zhang, Y.; Zheng, W.; Yao, Y.; Liu, Q.; Zhang, X.; Yang, Y.; Wang, X. Improved C-H Activation in Propane Dehydrogenation Using Zeolite-Stabilized Co-O Moieties. *ACS Catal.* **2023**, *13* (22), 14737−14745.
(43) Gomez, E.; Kattel, S.; Yan, B.; Yao, S.; Liu, P.; Chen, J. G. Combining CO_2 Reduction with Propane Oxidative Dehydrogenation over Bimetallic Catalysts. *Nat. Commun.* **2018**, *9* (1), 1398.
(44) Yue, Y.; Fu, J.; Wang, C.; Yuan, P.; Bao, X.; Xie, Z.; Basset, J. M.; Zhu, H. Propane Dehydrogenation Catalyzed by Single Lewis Acid Site in Sn-Beta Zeolite. *J. Catal.* **2021**, *395*, 155−167.
(45) Agbi, T.; Lo, W. S.; Baamran, K.; Ryu, T.; Cheung, C.; Rezaei, F.; Hermans, I. 3D-Printed Boron Nitride Catalytic Monoliths for Oxidative Dehydrogenation of Propane. *Top. Catal.* **2023**, *66*, 1152−1160.
(46) Nowicka, E.; Reece, C.; Althahban, S. M.; Mohammed, K. M. H.; Kondrat, S. A.; Morgan, D. J.; He, Q.; Willock, D. J.; Golunski, S.; Kiely, C. J.; Hutchings, G. J. Elucidating the Role of CO_2 in the Soft Oxidative Dehydrogenation of Propane over Ceria-Based Catalysts. *ACS Catal.* **2018**, *8* (4), 3454−3468.
(47) Qu, Z.; Sun, Q. Advances in Zeolite-Supported Metal Catalysts for Propane Dehydrogenation. *Inorg. Chem. Front.* **2022**, *9* (13), 3095−3115.
(48) Tian, H.; Liao, J.; Zha, F.; Guo, X.; Tang, X.; Chang, Y.; Ma, X. Catalytic Performance of In/HZSM-5 for Coupling Propane with CO_2 to Propylene. *ChemistrySelect* **2020**, *5* (12), 3626−3637.
(49) Tedeeva, M. A.; Kustov, A. L.; Pribytkov, P. V.; Kapustin, G. I.; Leonov, A. V.; Tkachenko, O. P.; Tursunov, O. B.; Evdokimenko, N. D.; Kustov, L. M. Dehydrogenation of Propane in the Presence of CO_2 on GaO_x/SiO_2 Catalyst: Influence of the Texture Characteristics of the Support. *Fuel* **2022**, *313*, 122698.
(50) Zhang, Y.; Aly, M. Effect of CO_2 on Activity and Coke Formation over Gallium-Based Catalysts for Propane Dehydrogenation. *Appl. Catal. A Gen.* **2022**, *643*, 118795.
(51) Djinović, P.; Zavašnik, J.; Teržan, J.; Jerman, I. Role of CO_2 During Oxidative Dehydrogenation of Propane Over Bulk and Activated-Carbon Supported Cerium and Vanadium Based Catalysts. *Catal. Lett.* **2021**, *151*, 2816−2832.
(52) Baek, J.; Yun, H. J.; et al. Preparation of Highly Dispersed Chromium Oxide Catalysts Supported on Mesoporous Silica for the Oxidative Dehydrogenation of Propane Using CO_2. *ACS Catal.* **2012**, *2* (9), 1893−1903.
(53) Wu, R.; Xie, P.; et al. Hydrothermally Prepared Cr_2O_3−ZrO_2 as a Novel Efficient Catalyst for Dehydrogenation of Propane with CO_2. *Catal. Commun.* **2013**, *39*, 20−23.
(54) Michorczyk, P.; Zeńczak, K.; Niekurzak, R.; Ogonowski, J. Dehydrogenation of Propane with CO_2-a New Green Process for Prope-Ne and Synthesis Gas Production. *Pol. J. Chem. Technol.* **2012**, *14* (4), 77−82.
(55) Gao, Y.; Jie, X.; Wang, C.; Jacobs, R. M. J.; Li, W.; Yao, B.; Dilworth, J. R.; Xiao, T.; Edwards, P. P. One-Pot Synthesis of Ca Oxide-Promoted Cr Catalysts for the Dehydrogenation of Propane Using CO_2. *Ind. Eng. Chem. Res.* **2020**, *59* (28), 12645−12656.
(56) Fu, H.; Qian, W.; Zhang, H.; Ma, H.; Ying, W. Different Alkali Metals Promoted Cr/Al_2O_3 Catalysts for Propane Dehydrogenation. *Fuel* **2023**, *342*, 127774.

https://doi.org/10.1021/acssuschemeng.4c06841
ACS Sustainable Chem. Eng. 2024, 12, 17783−17792